RESEARCH ARTICLE

The FASEB Journal

Transcriptional and functional regulation of cell cycle and UV response by PPARβ in human skin epidermal cells

Thanh Nhan Nguyen | Carine Winkler | Stefanie Ginster | Stéphanie Claudinot | Liliane Michalik | Paris Jafari

Center for Integrative Genomics, University of Lausanne, Lausanne, Switzerland

Correspondence
Paris Jafari, Centre for Integrative Genomics (CIG), University of Lausanne, UNIL-Sorge Génopode Building, CH-1015 Lausanne, Switzerland.
Email: paris.jafari@unil.ch

Abstract

Solar radiation is the main source of human exposure to UV rays, which is the major carcinogen in skin cancers by inducing DNA damage. Skin cells repair these damages by activating the DNA damage response (DDR) to safeguard genome integrity, thereby preventing skin cancers. Peroxisome proliferator-activated receptor beta (PPARβ), a druggable transcription factor, is involved in the development of UV-dependent skin cancers, although its role is not mechanistically elucidated. We showed previously that PPARβ knockout (KO) mice are less prone to UV-induced skin cancers. Here, we report that PPARβ directly regulates gene expression programs associated with cell cycle and DNA repair pathways in normal human epidermal keratinocytes (NHEK). The loss of function of PPARβ in human keratinocytes led to a downregulation in the expression of key cell cycle regulators, including cyclins and cyclin-dependent kinases (CDKs). Simultaneously, it upregulated the expression of p21 protein, a known CDK inhibitor. These molecular alterations resulted in a significant reduction in cell proliferation and induced cell cycle arrest at the G2/M phase. Moreover, the absence of functional PPARβ disrupted the expression and activation of the ataxia telangiectasia and Rad3-related (ATR) pathway, a critical component of the cellular response to UV-induced DNA damage. The alterations in the ATR pathway likely contributed to an increased apoptotic response of NHEK to UV radiation. Using a mouse melanoma model, we demonstrated that the depletion of PPARβ decreases tumorigenicity of melanoma cells and delays tumor formation. Our data suggest that PPARβ inhibition could be considered as a therapeutic target for the prevention of UV-induced skin cancers, by regulating cell proliferation,

attenuating DDR, and eliminating skin cells with high UV-induced mutational burden.

KEYWORDS

cell cycle, DNA damage response, keratinocyte, PPARβ, skin cancer, squamous cell carcinoma and UV

1 | INTRODUCTION

Ultraviolet (UV) radiation is the major environmental cause of the oncogenic transformation of human skin cells, leading to the development of skin cancers. UV induces DNA damage, genetic mutations, local immunosuppression, oxidative stress, and inflammation in skin cells, in the long term, can altogether contribute to photoaging and skin cancers.[1] Detection of UV-induced DNA lesions and recruitment of DNA repair molecules initiate the DNA damage response (DDR) in skin cells. DDR pathway is the key gatekeeper to protect the skin from damaging effects of UV radiation. UV-induced DNA damage primarily activates ataxia telangiectasia and Rad3-related (ATR) kinase protein that further phosphorylates p53 and cell cycle checkpoint kinase 1 (CHK1),[2] inducing cell cycle arrest[3] that allows time for DNA repair or eliminating cells with irreparable DNA lesions.[4] Unsuccessful DNA repair and persistent DDR activation can lead to cell death through apoptosis, thereby minimizing the risk for the proliferation of cell mutations. However, since the DDR-mediated DNA repair kinetics are slower than instant formation of DNA damage by UV,[5] some cells can continue DNA replication despite having unrepaired UV-induced lesions. Inhibition of DDR in rapidly proliferating cells such as cancer cells with high replication stress can lead to apoptosis,[6] and is considered as a therapeutic strategy with similar mechanism of action as in radiotherapy and DNA-damaging chemotherapeutics.[7] Inhibitors of ATR and CHK1, for example, can selectively kill cancer cells and potentiate the effect of DNA-damaging cancer therapies.[8–10]

Peroxisome proliferator-activated receptor beta (PPARβ) is a druggable ligand-dependent nuclear receptor and transcription factor, which has a role in regulating lipid and glucose metabolism in liver and skeletal muscles.[11] In mice, PPARβ also regulates keratinocyte homeostasis during skin wound healing.[12–16] We have demonstrated that PPARβ has a UV-responsive expression pattern in mouse skin, and both acute and/or chronic exposure to solar UV radiation cause an increased expression and activation of PPARβ in SKH-1 hairless mice.[17] Activation of PPARβ in mouse skin upon UV exposure increases the expression of the tyrosine kinase *Src*, an established proto-oncogene,[18] and induces an inflammatory response which provides a permissive environment for oncogenic transformation of cells.[19] We showed that genetic depletion or pharmacological inhibition of PPARβ significantly reduces the inflammatory response of mouse skin to UV exposure.[20] Along the same lines, PPARβ KO mice show a remarkably lower incidence of cancerous skin lesions in response to chronic UV exposure.[17] Herein, we investigate the role of PPARβ in the cellular response of human skin cells to UV radiation and explore the pathways that could link PPARβ to human skin cancers. We show that PPARβ has a regulatory effect on human keratinocyte proliferative capacity and cell cycle progression. We observe that PPARβ also controls the cellular response of human skin keratinocytes to UV radiation, by regulating the expression and activation of proteins involved in DDR. We pinpoint the ATR pathway of DDR to be controlled by PPARβ in response to UV-induced DNA damage and identify cyclin-dependent kinase inhibitor 1 (*CDKN1A*; p21) as a target regulated by PPARβ in response to UV. We also present proof-of-concept data on the efficiency of PPARβ depletion on reducing tumor growth in an in vivo melanoma xenograft model. As a ligand activated receptor with effective pharmacological inhibitors, PPARβ thus can be considered as a clinically relevant target for chemoprevention or treatment of UV-induced skin cancers.

2 | MATERIALS AND METHODS

2.1 | Cell culture, transfection, and treatments

Normal human epidermal keratinocytes (NHEK, A13401 Invitrogen), isolated from multiple neonatal foreskins were maintained in EpiLife™ Medium (MEPI500CA, Invitrogen) supplemented with human keratinocyte growth supplement (HKGS, S0015, Invitrogen), and penicillin–streptomycin 10 U/mL. Human squamous cell carcinoma cell line (SCC12, RRID:CVCL_4026), was kindly provided by Prof. Petra Boukamp (German Cancer Research Center, Heidelberg, Germany), and human squamous cell carcinoma cell line (SCC13, RRID:CVCL_4029), was kindly provided by Prof. Sabine Werner (Institute of Molecular Health Sciences, Zurich, Switzerland). The human squamous cell carcinoma lines, established from SCCs of the facial epidermis, were maintained in keratinocyte-SFM medium with

L-glutamine, EGF, BPE, and penicillin–streptomycin 10 U/ mL. Melanoma cell line, A375 (CLS Cat# 300110/p852_A-375, RRID:CVCL_0132) was cultured in DMEM growth medium (Gibco) supplemented with 4500 mg/L glucose, 10% fetal bovine serum, and penicillin–streptomycin 100 U/ mL. All the cell types were maintained in a humidified incubator at 37°C and 5% CO_2.

2.2 | Extraction of total RNA, reverse transcription, and real-time PCR

RNA extraction from cells in in vitro cultures was done using TRIzol reagent (Invitrogen) according to manufacturer's instructions. One microgram of total RNA was reverse transcribed using GoScript™ Reverse Transcriptase (Promega, A2801), following manufacturer protocol. Quantitative real-time PCR was performed with SYBR Green GoTaq® qPCR kit (Promega, A6002) using Stratagene Mx3000P thermocycler (5 min at 95°C then 40 cycles of 10 s at 95°C and 45 s at 60°C, then 1 min at 95°C, 30 s at 55°C and 30 s at 95°C). Primers were purchased from MicroSynth or Qiagen (primer sequences are presented in Table 1). mRNA expression was normalized to the expression of *EEF1A1 as* the housekeeping genes.

For in vivo experiments, the snap-frozen tumors were homogenized in TRIzol reagent using gentle MACS tubes (Miltenyi Biotec), and total RNA was isolated using Rneasy Mini Kit (Qiagen) and reverse transcribed as explained above. mRNA expression was normalized to the expression of both *EEF1A1* and *RPL27* genes, as housekeeping genes.

2.3 | RNA-seq experiment

NHEK cells were transfected with two different siRNA *PPARD* (siPPARD 2, siPPARD D), or control siRNA in three independent experiments. Seventy-two hours following siRNA transfection, RNA samples were extracted using RNeasy Mini Kit (74104 Qiagen), and technical replicates (three) of the same condition were pooled. RNA-seq experiment was conducted at the Lausanne Genomic Technologies Facility (Lausanne, Switzerland) according to an in-house pipeline. Briefly, the RNA quality was

TABLE 1 Primer sequences.

Primer	Sequence (forward)	Sequence (reverse)
ANGPTL4	GAC CTC AGA TGG AGG CTG GA	AAG TCC ACT GAG CCA TCG TG
CCNB1	GAT TGG AGA GGT TGA TGT CGA GCA A	GTG CTA AGC AAA AAG CTC CTG CTG
CCND1	AAG TGT GAC CCG GAC TGC CTC C	GCA CGT CGG TGG GTG TGC AAG
CDKN1A	CTG TCA CTG TCT TGT ACC CT	GGT AGA AAT CTG TCA TGC TGG
IL1b	GCACGATGCACCTGTACGA	AGAACACCACTTGTTGCTCCATATC
PPARD	GCATGAAGCTGGAGTACGAGAAG	GCATCCGACCAAAACGGATA
PPARA	ACGATTCGACTCAAGCTGGT	CGACAGAAAGGCACTTGTGA
PPARG1	AAGGCCATTTTCTCAAACGA	AGGAGTGGGAGTGGTCTTCC
EEF1A1	TCTCAGGCTGACTGTGCTGT	CACCCAGTGTGTAAGCCAGA
RPL27	GTGAAAGTGTATAACTACAATCACC	TCAAACTTGACCTTGGCCT
E2F1	CCG CCA TCC AGG AAA AGG TGT GAA	AGG TCG ACG ACA CCG TCA GC
MCM2	GGTACTGCTATGGCGGAATCA	TGGAGGTGAGGGCATCAGTA
MCM3	GCTGTCACGATTTGACTTGCT	AAGGGCATAGCATCGCCA
MCM4	CAGGCTCTCATCGAGGCTTAT	TAGCTGTCGAGGGTATGCAG
MCM5	ACTTCACCAAGCAGAAATACCC	CGAGTCCATGAGTCCAGTGAG
MCM6	TGATAAGATGGACGTGCGGG	GGCGTTCAGAGTAGCCTTCA
MCM7	AGCTTCAATCGCCCCAGAAA	ATGTTGATGTTGCCCCGGAT
FANCA	GACCTGAATGCCCTTTTGCT	ATCCTGCAAAGCAGAGCCTAT
FANCCD2	AGGAGACACCCTTCCTATCCC	AAGATGCACCCATACTGGCTT
FANCI	ACTGCCCTGGCTACGAAAAA	TATTGCTGATCCCACCTGCC
BRCA2	ACCCAGCTTACCTTGAGGGTT	AGCAGATTCCATGGCCTTCC
CDC20	AATGTGTGGCCTAGTGCTCC	CACCATGCTACGGCCTTGA
CDC25B	CAGAAACGATGGTGGCCCTA	AGTTCACCGCAGTCTTGATGT
CDC45	CACCAACCTCGTCATCTCCC	GCCGGTTCTTTGTCGAACAC

assessed on a Fragment Analyzer (Agilent Technologies) and all RNAs had a RQN from 9.2 to 10. RNA-seq libraries were prepared from 500 ng of total RNA with the Illumina TruSeq Stranded mRNA reagents (Illumina) using a unique dual indexing strategy and following the official protocol automated on a Sciclone liquid handling robot (PerkinElmer). Libraries were quantified by a fluorimetric method (QubIT, Life Technologies) and their quality assessed on a Fragment Analyzer (Agilent Technologies). Sequencing was performed on an Illumina NovaSeq 6000 for 100 cycles single read. Sequencing data were demultiplexed using the bcl2fastq2 Conversion Software (version 2.20, Illumina).

2.4 | RNA-seq data processing

Data cleaning: Purity-filtered reads were adapters and quality trimmed with Cutadapt (v. 1.8, Martin 2011). Reads matching to ribosomal RNA sequences were removed with fastq_screen (v. 0.11.1). Remaining reads were further filtered for low complexity with reaper (v. 15-065). Reads were aligned against the GRCh38.102 genome using STAR (v. 2.5.3a). The number of read counts per gene locus was summarized with htseq-count (v. 0.9.1) using GRCh38.102 gene annotation. Quality of the RNA-seq data alignment was assessed using RSeQC (v. 2.3.7). Statistical analysis was performed in R (R version 4.1.0). Genes with low counts were filtered out according to the following rule: at least 1 sample had to have a at least1 cpm (1 count per million) reads in order to keep the gene in the dataset. Library sizes were then scaled using TMM normalization. Subsequently, the normalized counts were transformed to cpm values and a log2 transformation was applied by means of the function cpm with the parameter setting prior. counts = 1 (EdgeR v 3.34.1).

2.5 | Differential expression

Differential expression was computed with the R Bioconductor package limma by fitting data to a linear model and employing the limma-trend approach. This method was selected due to its robustness for datasets with consistent sequencing depth across samples. In our study, the read counts per library ranged from 16 128 506 to 22 233 245, representing a 1.4-fold difference, which is well within the recommended range for effective application of limma-trend. Results from contrasts of interest and interactions were extracted. Moderated F-tests were performed for groups of contrasts and groups of interactions. The resulting p-values were adjusted for multiple testing by the Benjamini–Hochberg method, which controls for the false discovery rate (FDR). This adjustment was performed for each F-test. A post-hoc test was performed, using the function decideTests with parameter method = nestedF.

2.6 | Lentivirus packaging, titration, and transduction

For gene knockdown experiments, the shRNA transfer plasmids for *PPARD* were obtained from the Mission TRC library (Sigma, TRCN0000001661 and TRCN0000010647). Lentiviruses were produced as described previously.[21] Briefly, the two helper plasmids (package and envelope) and the shRNA transfer plasmids were transfected in 293T cells using a calcium phosphate-based method. Forty-eight hours post-transfection, the supernatants containing lentiviruses were collected, filtered, and stored at −80°C as aliquots. A375 cells were seeded and incubated with viral stocks supplemented with 4 μg/mL Polybrene for 16 h and then supplied with fresh medium. Forty-eight hours post-transduction, transduced cells were selected and maintained with puromycin at 1 μg/μL concentration.

2.7 | siRNA transfection

To knockdown the expression of PPARβ in NHEK, SCC12, and SCC13 cells, we applied siRNA constructs against human *PPARD*. We used a scrambled siRNA construct (ON-TARGETplus Non-targeting Control Pool, D-001810-10-20, Horizon Discovery) as a negative control for PPARD downregulation. siRNAs transfection was done at the concentration of 10 nM using the Lipofectamine RNAimax (Invitrogen), for 6 h. The cells were then washed, and the media were replaced with fresh media. For NHEK, six individual siRNAs obtained from two different suppliers (Horizon Discovery and Sigma) were tested for their PPARβ knockdown efficacy at the mRNA and protein levels. Based on these assessments, two individual siRNAs were selected as following: siPPARD D (J-003435-09, Horizon Discovery) and siPPARD 2 (Hs01_00236947, Sigma). For other cells, a pool of siPPARD targeting constructs were used.

2.8 | UVB exposure

UVB exposure was done with an intensity of 30 mJ/cm^2 in cells grown in six-well plates, using a BIO-SUN ++ Microprocessor-controlled, cooled UV irradiation system (Vilber).

2.9 | Pharmacological inhibition of PPARβ

Cells were treated with vehicle DMSO or PPARβ antagonist GSK0660 (MedChemExpress, HY-12377) at a final concentration of 0.5 μM for 24 h prior to UVB exposure and kept under GSK0660 treatment for the duration of the experiment.

2.10 | Cell proliferation assays

Cells were seeded in 96 wells plate and transfected with *PPARD* siRNA (or control siRNA) or treated with vehicle or GSK0660 and assessed for proliferation after 72 h, using Click-iT™ EdU Proliferation Assay kit for Microplates (Invitrogen, C10499) following manufacturer's protocol. In brief, cells were incubated with 10 μM EdU for 4 h, before being fixed, washed, and stained with 1X Click-iT™ reaction cocktail and subsequently with Amplex™ UltraRed reagent.

DNA synthesis as an indicator of cell proliferation was measured by quantifying the fluorescence signal (excitation 548 nm, emission 605 nm) analyzed with a TECAN spectrophotometer (Männedorf, Switzerland). All results represent the mean $\pm$ SD of three to four independent experiments done in three technical replicates.

2.11 | Colony-forming assays

Control or stably expressing shPPARD melanoma cells (A375; 10^3 cells/well) were seeded in 6-well plates and cultured for 2 weeks until the colonies were formed. Formed colonies were washed twice with $1 \times$ PBS, fixed by 4% paraformaldehyde, and stained with 0.5% crystal violet. Six well plates were imaged by digital camera and colonies were counted using ImageJ software.

2.12 | CPD ELISA assay

NHEK cells transfected with siRNA control or siRNA against *PPARD* were exposed to UVB radiation and harvested at 0 h (immediately after UV exposure), 1 h, 6 h, 24 h, and 48 h post-exposure. DNA from these cells was extracted using the Wizard® Genomic DNA Purification Kit (Promega, A2361). The DNA samples at 50 ng/ μl diluted in TE buffer (10 mM Tris, 1 mM EDTA, pH 8) were converted to single-strand DNA by heat denaturing for 10 min at 95°C and subsequently chilling on ice for 10 min and then absorbed onto a 96-well DNA high-binding microplate. The detection of the CPD was performed with

an OxiSelect UV-Induced DNA Damage ELISA Kit (Cell Biolabs Inc., STA-322) following the manufacturer's instructions. The CPDs in the sample or standard were probed with an anti-CPD antibody, followed by a Horse Radish Peroxidase-conjugated secondary antibody. Absorbance was read at 450 nm using a Biotek machine for the UVB-exposed samples and nonirradiated controls.

2.13 | Flow cytometry assay to analyze cell the cycle

Cells were cultured in 6-well plates, and then transfected with *PPARD* siRNA (or control siRNA) or treated with vehicle or GSK0660 for 48 h. Then incubated with 10 μM EdU for 1 h at 37°C, and then detached and fixed with 4% paraformaldehyde solution. EdU incorporation was determined with the Click-iT EdU Alexa Fluor 647 flow cytometry assay kit (Invitrogen, C10424) according to the manufacturer's instructions. Briefly, cells were washed twice in 1× saponin-based permeabilization and wash reagent and stained with the Click-iT EdU reaction cocktail (1×). Samples were incubated for 30 min at room temperature in the dark and washed with 1× saponin-based permeabilization and wash reagent. DNA was stained by incubating with saponin-based permeabilization and wash buffer containing 0.2 mg/mL RNase and 5 μg/mL Propidium Iodide. Cells were then acquired using Accuri C6 flow cytometer (BD Accuri C6 Plus, RRID:SCR_014422) and analyzed using FlowJo™ v10.7.1 Software (FlowJo, RRID:SCR_008520).

2.14 | Apoptosis analysis

Cells treated grown in 6-well plates and exposed to UVB (30 mJ/cm^2). The rate of apoptotic response was measured at 48 h after UV exposure using eBioscience™ Annexin V Apoptosis Detection Kit APC (Invitrogen, 88-8007), following the manufacturer's instructions. Briefly, cells were trypsinized and washed with 1× binding buffer before being stained with fluorochrome-conjugated Annexin V diluted in 1× binding buffer for 15 min at room temperature. Subsequently, cells were washed and stained with propidium iodide (PI), then analyzed with Accuri C6 flow cytometer (BD Biosciences) and analyzed using FlowJo™ v10.7.1 Software (Tree Star, Inc).

2.15 | Western blot analysis

Cells were lyzed in RIPA buffer (containing 50 mM Tris [pH 7.4], 150 mM NaCl, 0.1% SDS, 1% NP-40, 0.5% sodium

deoxycholate), supplemented with Protease/Phosphatase Inhibitor Cocktail 1× (5872S, Cell Signaling). Protein amount was quantified using Pierce™ BCA Protein Assay Kit (23225, Life Technologies). After quantification, proteins (15–20 μg per well) were separated by SDS-PAGE and subjected to immunoblotting. All primary antibodies were incubated overnight in 1× Tris-buffered saline plus 0.1% Tween-20 and 5% bovine serum albumin or 5% nonfatty milk at a dilution recommended by the manufacturer, followed by peroxidase conjugated goat anti-mouse or anti-rabbit secondary antibodies (Promega W402B or W401B). Immunoreactivity was detected using Advansta ECL WesternBright Quantum (ref K-12042-D20) or Amersham™ ECL Select™ Western Blotting Detection Reagent (ref RPN2235). Images were acquired using a Fusion fx (Vilber). Anti-CHK1 (Cell Signaling Technology Cat# 2360, RRID:AB_2080320), Anti-CHK2 (Cell Signaling Technology Cat# 3440, RRID:AB_2229490), anti-phospho CHK1 Ser 345 (Cell Signaling Technology Cat# 2348, RRID:AB_331212), anti-phospho CHK2 Thr68 (Cell Signaling Technology Cat# 2197, RRID:AB_2080501), anti-p21 (Cell Signaling Technology Cat# 2947, RRID:AB_823586), anti-gH2AX (Cell Signaling Technology Cat# 2577, RRID:AB_2118010), anti-Cyclin B1 (Cell Signaling Technology Cat# 12231, RRID:AB_2783553), anti-phospho p53 Ser15 (Cell Signaling Technology Cat# 9286, RRID:AB_331741), anti-GAPDH (Cell Signaling Technology Cat# 2118, RRID:AB_561053). anti-p53 (Santa Cruz Biotechnology Cat# sc-126, RRID:AB_628082), anti-PPARβ (Santa Cruz Biotechnology Cat# sc-74 517, RRID:AB_1128604), anti-E2F1 (Santa Cruz Biotechnology Cat# sc-251, RRID:AB_627476), anti-Actin (Sigma-Aldrich Cat# A2066, RRID:AB_476693).

2.16 | Animal experimentation

All experiments involving animals were approved under the number VD1528 by the Veterinary Office of the Canton Vaud (Switzerland) in accordance with the Federal Swiss Veterinary Office Guidelines and conform to the Commission Directive 2010/63/EU. Mice were raised, housed, and experienced in the conventional animal facility of the Centre for Integrative Genomics, at the University of Lausanne. They were kept on IVC cages in a standard colony (2–5 animals per cage), in a light-controlled environment (12/12-h light/dark cycle, artificial light with daylight spectrum at an average intensity of 100 lx), with a hygrometry between 45% and 65% and a temperature of 22°C (±2°C). They were housed on Aspen bedding (Safe select) and fed ad libitum with Sp-150 irradiated pellets (Safe) and filtered water.

Tumor growth in vivo: Nude mice (Rj: NMRI-$Foxn1^{nu/nu}$, RRID:IMSR_RJ:NMRI-NUDE) were ordered from Janvier Labs (France). 1×10^6 cells of shscb or shP-PARD-A375 were injected into the left flank of 10-week-old or older female mice in compliance with the University of Lausanne Institutional regulations. Mice behavior and tumor growth were monitored twice a week. The maximum volume authorized by the authorities was fixed at $1 cm^3$, thus mice were sacrificed when the interruption criteria (tumor size more than $1 cm^3$) were reached, and the tumors were recovered for further analysis.

2.17 | Statistical analysis

Statistical analysis and graph construction were performed in GraphPad Prism (version 9.4.0). Results are presented as mean values ± standard deviation. Two-tailed Student's t-test for two group comparisons, and one-way ANOVA with Dunnett's multiple-comparison test, or two-way ANOVA with Tukey's multiple-comparison test was applied for more than two group comparisons. Probability was considered to be significant at $p < .05$.

3 | RESULTS

3.1 | Transcriptome profiling reveals that PPARβ has a transcriptional regulatory function on cell cycle and DNA repair in human epidermal keratinocytes

To investigate the role of PPARβ in transcriptional control of cellular functions in human keratinocytes, we measured global changes in transcriptome as a consequence of siRNA-mediated PPARβ depletion in NHEK, by RNA-seq analysis. PPARβ depletion was achieved by separately introducing two small interfering RNAs (siRNAs; siPPARD D and siPPARD 2) targeting two different sequences of *PPARD* mRNA (gene encoding PPARβ) into NHEK cells. While siPPARD D and siPPARD 2 led to an average downregulation of 50 and 80% (respectively) in the expression of *PPARD* mRNA, the expression of the two other PPAR isoforms remained unchanged (PPARα and PPARγ). PPARβ depletion was also confirmed at the protein level (Figure S1).
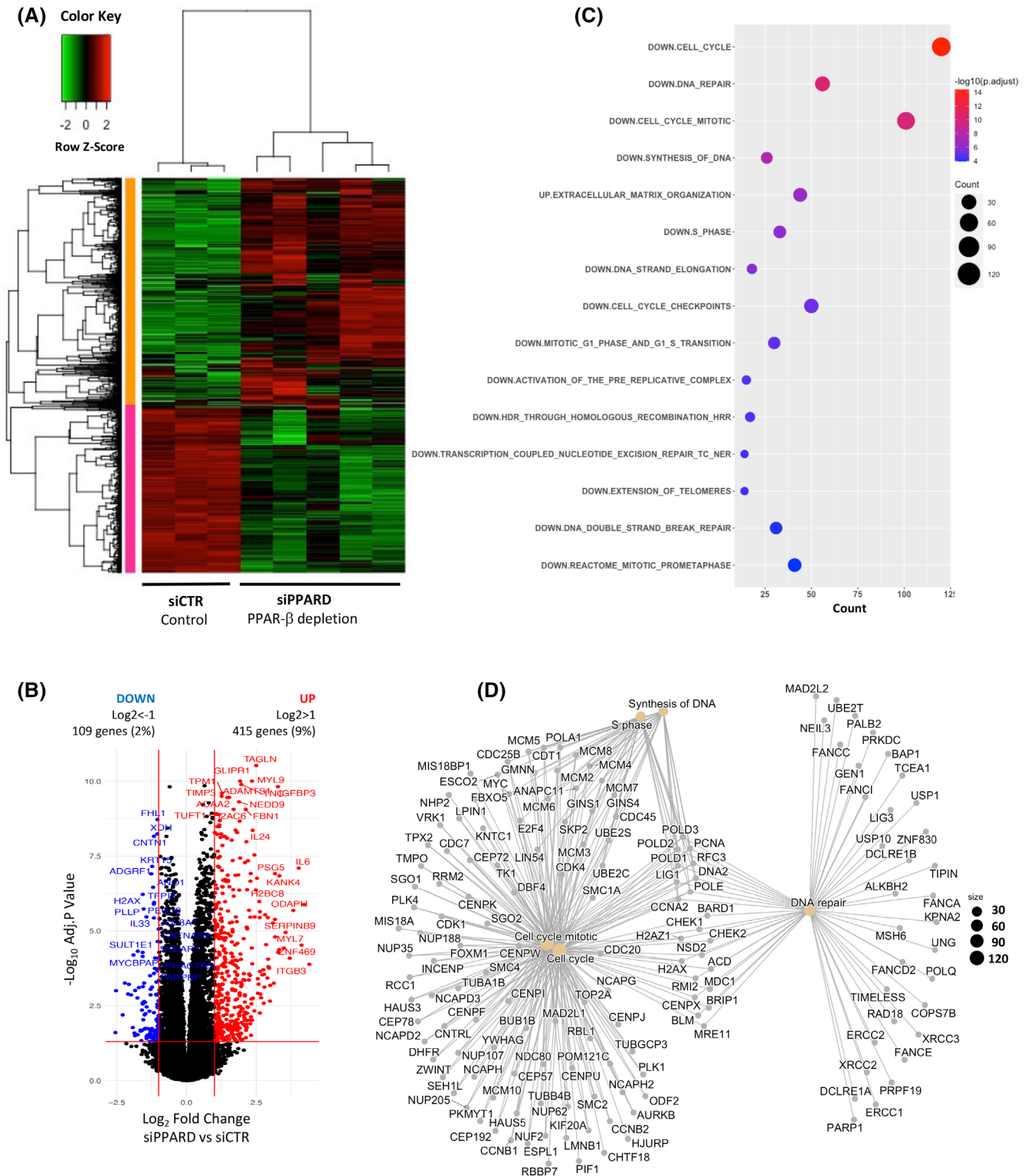
PPARβ depletion using each of the individual siRNAs resulted in significant transcriptional changes in NHEK cells as revealed by RNA-seq. For further analysis of the RNA-seq data, we selected only those genes exhibiting similar direction of changes in expression (significantly up or downregulation) with both siRNAs, as a way to enrich in bona fide PPARβ-regulated genes and eliminate off-target effects. A

total of 4430 differentially expressed genes (DEGs, adjusted *p*-value <.05) relative to control NHEK cells were thereby identified (Figure 1A). Among those, 109 genes were significantly downregulated, and 415 genes were significantly upregulated at least twofold compared to control NHEK cells (Figure 1B). Pathway enrichment analysis of these DEGs revealed that among the 15 most enriched pathways, 14 were downregulated and one upregulated (Figure 1C). The two most highly enriched pathways were "cell cycle" and "DNA repair", which were both downregulated. Of note, not only the top-two but all the downregulated enriched pathways were related to the regulation of cell cycle or to DNA maintenance (Figure 1C; enriched pathways include synthesis of DNA, S phase, DNA strand elongation, cell cycle checkpoints, mitotic G1 phase and G1-S transition, transcription coupled nucleotide excision repair, double strand break repair), as also illustrated by the visualization of gene interaction network (Figure 1D).

We then took a closer look at DEGs assigned to the "cell cycle" and "DNA repair" (Reactome Pathway Database) using a heatmap representation, which clearly showed downregulation of the expression of these genes in response to PPARβ depletion in NHEK cells (Figure 2A). Moreover, gene set enrichment analysis (GSEA) showed that the transcriptome changes of PPARβ-depleted NHEK cells compared to the Molecular Signatures Database (MSigDB) hallmark gene sets, were most significantly correlated with the gene signature of G2M checkpoint dataset (FDR *Q*-value = 0.0 and normalized enrichment score [NES] = −2.5) and E2F family of transcription factor target dataset (FDR Q-value = 0.0 and normalized enrichment score [NES] = −2.85), (Figure 2B, top and bottom panels, respectively). E2F is a major family of transcription factors that regulates cell cycle and proliferation.[22] To consolidate these analyses, we further quantified the expression of genes involved in cell cycle progression following siRNA-mediated PPARβ depletion in NHEK cells using real-time qPCR, in additional independent experiments. This included the minichromosome maintenance protein complex (MCM) gene family (*MCM2-7*).[23] The expression of *MCM2-7* genes was strongly downregulated in PPARβ-depleted NHEK cells, with amplitudes ranging from 25% (*MCM3*, *MCM4*) to 60% (*MCM2, MCM5*) (Figure 2C, top left panel). The expression of other major cell cycle regulators (*CCNB1*, *CDC20*, *CDC25B*, and *CDC45*; Figure 2C, top right panel), and DNA repair regulators (genes of the Fanconi Anemia/BRCA (FA/BRCA) pathway including *FANCA*, *FANCD2*, *FANKI*, and *BRCA2*; Figure 2C, bottom panel) was also downregulated upon PPARβ depletion. Together, these results demonstrate the transcriptional regulatory function of PPARβ on the expression genes that are major regulators of cell proliferation and DNA repair processes.

3.2 | PPARβ functionally regulates cell proliferation and cell cycle progression in normal and malignant human keratinocytes, and melanoma cells

Pathway enrichment analysis of transcriptomic profiles in our RNA-seq data, followed by real-time qPCR quantification of gene expression in independent biological samples showed that PPARβ depletion in NHEK cells caused transcriptional repression of genes involved in the regulation of cell cycle (Figures 1 and 2). We therefore assessed whether this had functional consequences in normal and malignant epidermal cells. We depleted PPARβ from NHEK cells by siRNA-mediated gene silencing. Consistent with the transcriptional regulation of genes involved in the control of cell cycle, depletion of PPARβ in NHEK cells dramatically reduced their proliferation (92 ± 6% by siPPARD D, and 94 ± 2.5% by siPPARD 2), as shown by decreased DNA synthesis quantified by EdU uptake (Figure 3A, left panel). Detailed FACS analysis of cell cycle progression showed that PPARβ depletion caused a significant decrease in the proportion of cells in S phase (41 ± 7% and 83 ± 4% decrease in the percentage of cells in the S phase as compared to control, by siPPARD D and siPPARD 2, respectively), and an accumulation of cells in the G2/M phase in NHEK keratinocytes (32 ± 11% and 64 ± 7% increase in the percentage of cells in the G2/M phase as compared to control, by siPPARD D and siPPARD 2, respectively). These data suggest a G2/M cell cycle arrest (Figure 3A, right panel), consistent with the observed downregulation of G2/M transition regulators *CCNB1* and *CDC25B* (Figure 2B,C). In addition to cyclins (mainly cyclin D, cyclin E, cyclin A, or cyclin B) and cyclin-dependent kinases (CDKs; *CDK4*, *CDK6*, *CDK2*, or *CDK1*),[24] which were all revealed to be downregulated in PPARβ-depleted cells through RNA-seq data (Figure 3B), cell cycle is also regulated by the activity of cyclin-dependent kinase inhibitors.[25] Transcriptome analysis revealed an upregulation of p21 gene (*CDKN1A*; Figure 3B), which is a crucial cell cycle regulator in particular following DNA damage, by inhibiting CDKs and blocking the cell cycle progression.[26] We indeed, could confirm the increased expression of p21/*CDKN1A* upon PPARβ depletion in NHEK cells in independent experiments at mRNA (1.51 ± 0.22 and 1.87 ± 0.16-fold increase compared to control, by siPPARD D and siPPARD 2, respectively; Figure 3C, left), and protein levels (1.8 ± 0.4 and 2.1 ± 0.2-fold increase compared to control, by siPPARD D and siPPARD 2, respectively; Figure 3C, right). Similarly, PPARβ depletion from malignant human keratinocytes (Squamous Cell Carcinoma cells, SCC13) and invasive human melanoma cells (A375) using a pool of four siRNAs (Figure S1, top and bottom panel, respectively), led

(A) Color Key

siCTR
Control

siPPARD
PPAR-β depletion

(C)

(B)

DOWN
Log2<-1
109 genes (2%)

UP
Log2>1
415 genes (9%)

(D)

to reduced proliferation (around 26%) in these cells as measured by the percentage of EdU uptake (Figure 3D). Unlike healthy NHEK cells however, which exhibited an accumulation of cells in the G2/M phase, FACS analysis of cell cycle progression revealed a slight accumulation of SCC13 and A375 cells at the G1 phase, concomitant with the decrease in the number of cells at the S phase,

suggesting a G1/S transition arrest (Figure 3D). Similar results were obtained with siRNA-mediated depletion of PPARβ in an additional human malignant cells line of keratinocyte origin (SCC12; Figure S2). These data report that the expression changes in genes regulating cell cycle and proliferation following PPARβ depletion, are translated into functional changes in these cellular processes,

confirming a cell cycle regulatory role for PPARβ in human skin keratinocytes. However, the regulation of the cell cycle by PPARβ in healthy and malignant cells appears to be different.

3.3 | PPARβ-depletion regulates the UV response in normal human keratinocytes

To cope with various types of genotoxic stress including UV radiation, cells activate response mechanisms to DNA damage, which includes cell cycle arrest, DNA repair, and apoptosis to maintain the genome integrity.[27] The data we collected so far strongly suggest that this DDR may be affected in skin cells depleted of PPARβ (Figures 1 and 2). We therefore tested this hypothesis by comparing the responses of PPARβ-depleted and control NHEK cells to DNA damage induced by exposure to UVB radiation (30 mJ/cm^2). Induction of DNA damage was evidenced by the measurement of the UV-induced CPD lesions, that did not significantly differ between PPARβ-depleted and control NHEK cells (Figure S3). We then studied the activation of major DDR proteins in UVB irradiated NHEK cells starting with H2AX, which its phosphorylation is a key initiating step in the DDR. Phosphorylated H2AX, known as γH2AX, has a sensory function for DNA damage and is one of the early initiators of DDR.[28,29] As expected, UVB exposure led to a significant increase in γH2AX detection in NHEK cells (Figure 4A). The phosphorylation, and thereby activation, of H2AX was strongly affected only in cells in which PPARβ depletion was achieved with siPPARD 2 (Figure 4A), the siRNA that causes the greatest decrease in PPARβ (80% decrease, Figure S1). In these cells, we observed a 0.34 ± 0.04-fold decrease in H2AX phosphorylation compared to control by siPPARD 2, at 6 h post UV exposure. NHEK cells with siPPARD D-mediated PPARβ depletion (50% decrease, Figure S1) did not show a significant reduction in H2AX phosphorylation. Downstream in the DDR, among the two major kinases that respond to the genotoxic stress ATM and ATR, ATR plays a prominent role in response to UV radiation by phosphorylating p53 and the checkpoint kinases

CHK1 and CHK2, thereby activating them.[30] Activation of these DDR effector proteins leads to the inhibition of cyclin-dependent kinase activity and the blockage of the cell cycle progression, allocating cells enough time to repair the DNA damage.[31,32] Therefore, we asked whether PPARβ depletion could affect the ATR/ATM-mediated response to UV-induced DNA damage. We examined the expression, and phosphorylation of the ATR/ATM-dependent kinases including the serine 345 residue of CHK1, threonine 68 of CHK2,[2,33] and serine 15 of p53,[34] that leads to their activation, in the control and PPARβ-depleted NHEK cells. As expected, UVB exposure (30 mJ/cm^2) in control NHEK (siCtrl pool) induced the phosphorylation of both CHK1 and CHK2 at 0.5 h, that peaked at 2 h post-exposure (Figure 4B, top and middle panels, respectively). siRNA-mediated PPARβ depletion led to a decrease both in the expression of CHK1 protein, and also its phosphorylation at 0.5, 2, and 6 h post UVB exposure (Figure 4B; top panel). This effect was more prominent in cells treated with siP-PARD 2, which induces a stronger reduction in PPARβ expression (80% downregulation vs. 50% downregulation induced by siPPARD D). The impact of PPARβ depletion on CHK2 was less prominent and only a slight attenuation of phosphorylation at 2 h post UVB exposure was observed (Figure 4B; middle panel). Regarding p53, the peak of p53 phosphorylation was detected at 6 h post UVB exposure in control NHEK cells, whereas the depletion of PPARβ with siPPARD 2 prevented maximal activation of p53 through reducing both its expression and phosphorylation (Figure 4B; lower panel).

As shown in Figure 3C, our global expression analysis of PPARβ-depleted human normal keratinocytes followed by western blot quantification revealed that PPARβ depletion resulted in increased expression of p21. In addition to its role as a cell-cycle inhibitor described above, p21 is also involved in modulating DDR through a CDK-independent pathway and by playing a role in DNA repair through its interactions with multiple DNA repair factors.[35,36] We thus further examined the impact of PPARβ depletion on the expression of p21 in UV-exposed human keratinocytes. As shown earlier in

FIGURE 1 PPARβ regulates the transcription of genes involved in cell proliferation and DNA repair in NHEK cells. (A) Differentially expressed gene (DEGs) clustering heatmap for RNA-seq data showing the log2 transformed normalized expression values of PPARβ-depleted samples (right, siPPARD, $n = 5$), and controls (left, siCTR, $n = 3$), each row representing one gene. Log2 expression values for each gene are resized to row z-score scale (from -2, the lowest expression to $+2$, the highest expression) and colors represent gene expression changes (Red, upregulation and green, downregulation). (B) Volcano plot showing differentially expressed genes in PPARβ-depleted (siPPARD, $n = 5$) compared to control NHEK cells (siCTR, $n = 3$). The genes with significant changes in expression (adjusted p-value $<.05$ and an absolute value of log2 fold change >1) are colored in red (upregulated) or blue (downregulated). (C) Bubble plots showing top significantly enriched pathways for differentially expressed genes in PPARβ-depleted cells compared to controls as determined by reactome pathway enrichment analysis. The top 15 enriched pathways are visualized according to the gene count (size of circles), and $-$log10 adjusted p-value $<.05$ (color of circles) (D) cNET plot of the top five enriched biological processes of downregulated genes in PPARβ-depleted cells as compared to controls. The size of the nodes correlates with the number of enriched DEGs.
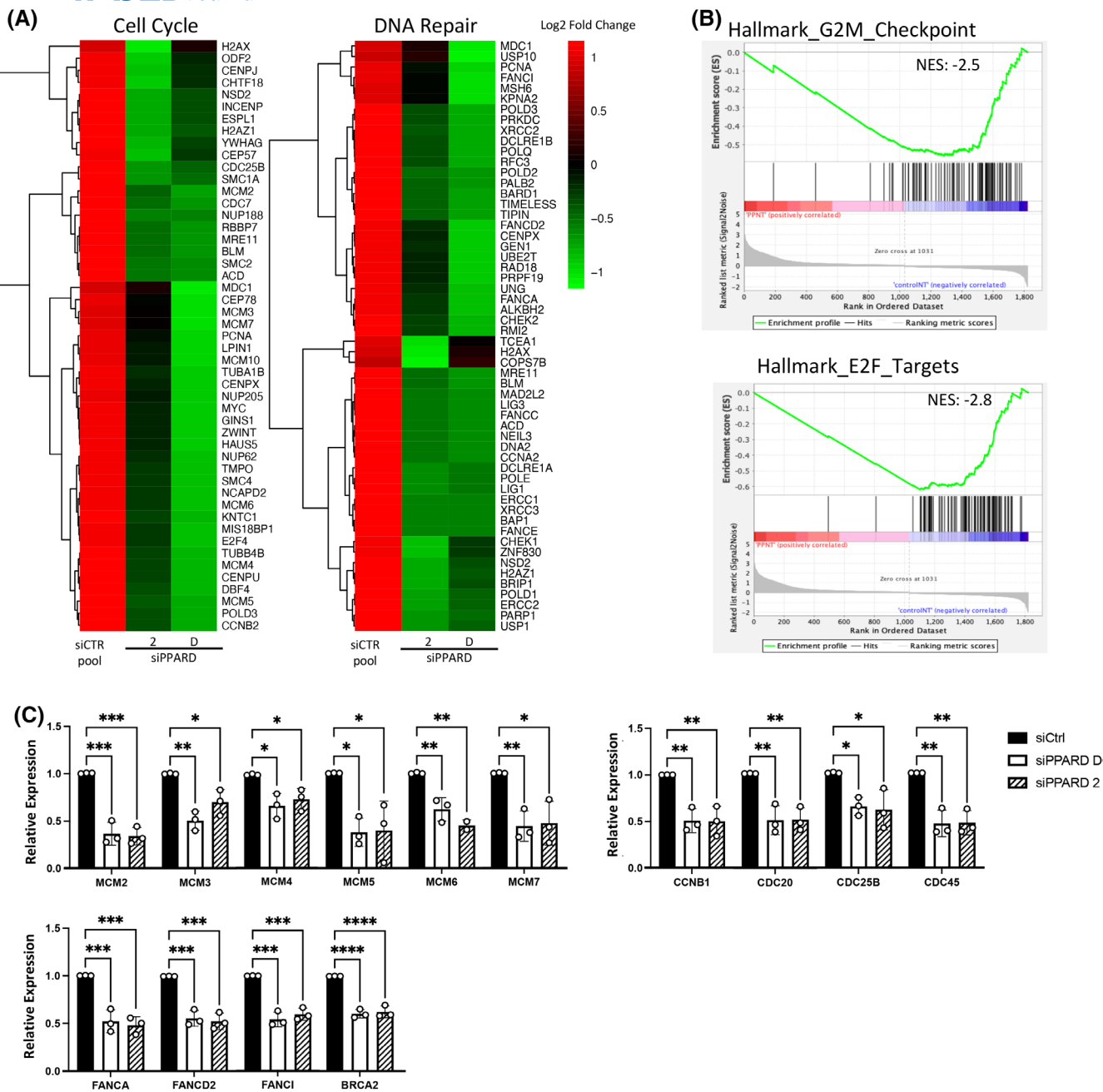
FIGURE 2 Depletion of PPARβ leads to a downregulation of the cell cycle and DNA repair pathways. (A) Heatmaps showing the mean of log2 transformed expression values of genes regulating cell cycle (left) and DNA repair (right), in PPARβ-depleted samples (two independent siRNA: SiPPARD 2; siPPARD D, $n = 3$ for each) compared to control (siCTR pool, $n = 3$). Each row represents one gene, and log2 expression values for each single gene are resized to row z-score scale (from -1, the lowest expression to $+1$, the highest expression for single gene) and colors represent gene expression changes. Red indicates upregulation of gene expression and green indicates downregulation of expression. (B) GSEA analysis of DEGs following PPARβ depletion. (C) Quantification of the expression of selected genes belonging to cell cycle and DNA repair pathways quantified by qPCR in control (siCtrl) and PPARβ-depleted (siPPARD D, siPPARD 2) in normal human epidermal keratinocytes (NHEK). Bars represent mean $\pm$ standard deviation from three independent biological replicates (white circles), each with three technical replicates. (***$p < .001$; **$p < .01$; *$p < .05$, one-way ANOVA with Dunnett's multiple-comparison test).

Figure 3C, the expression of p21 increased two-fold in PPARβ-depleted NHEK cells compared to controls in the absence of UV exposure (Figure 4C; compare time 0). In control NHEK cells (siCtrl pool), UVB exposure caused a progressive reduction in the p21 protein between 0.5-,

and 6-h post-exposure (Figure 4C), in line with studies showing that UV-induced p21 degradation in an ATR-dependent manner is essential for DNA repair.[37,38] In PPARβ-depleted cells the reduction in p21 protein levels in response to UV exposure was also observed. However,
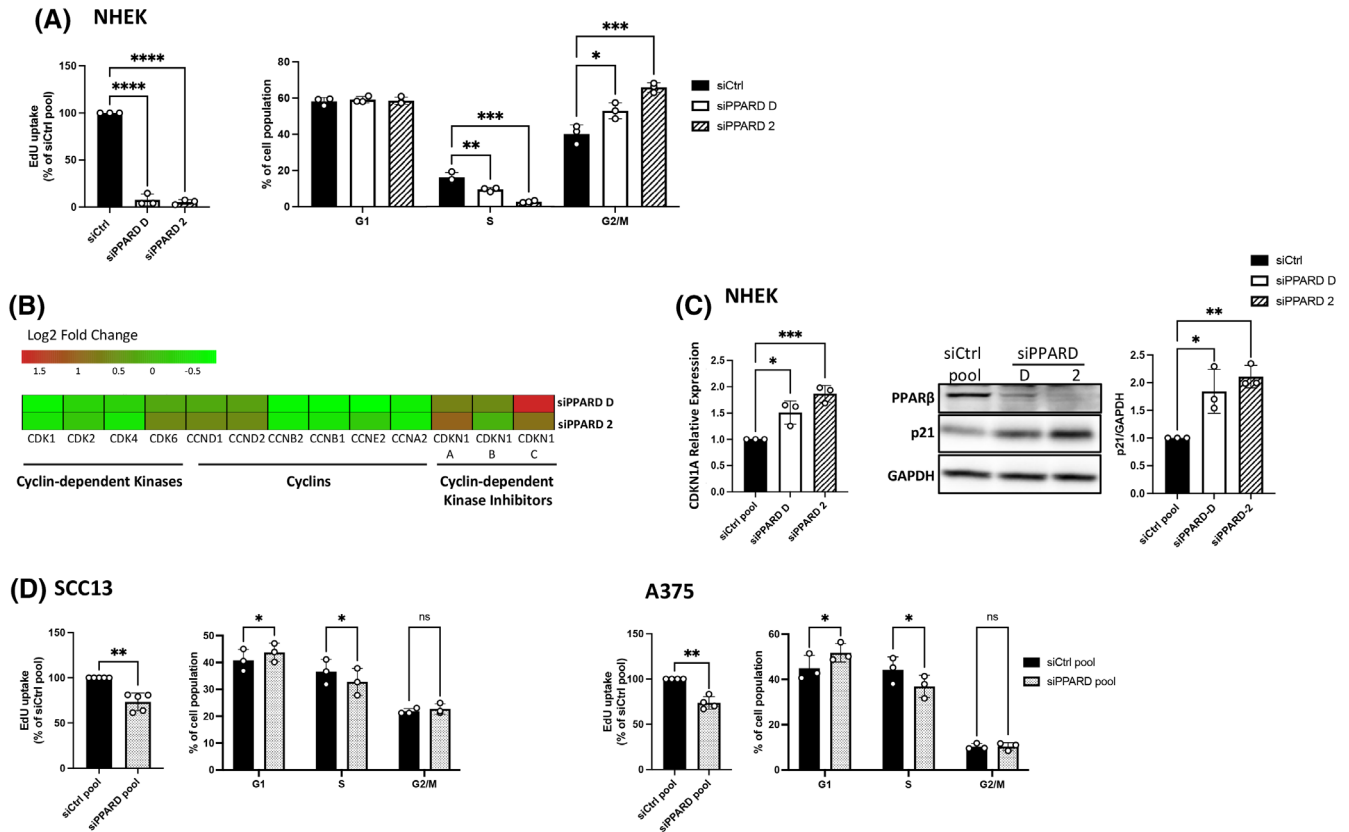
FIGURE 3 Impact of PPARβ depletion on cell proliferation and cell cycle progression. (A) Cell proliferation quantified using EdU uptake (left panel), and FACS analysis of the cell cycle progression (right panel) in normal human epidermal keratinocytes (NHEK), 72 h after transfection with control (siCtrl) or two different *PPARD* siRNAs (siPPARD D, siPPARD 2). (B) Heatmap of the log2 fold changes in expression of the genes directly involved in the control of cell cycle in NHEK cells, 72 h after transfection with control (siCtrl) or two different *PPARD* siRNAs (siPPARD D, siPPARD 2). (C) Expression of p21 at mRNA (CDKA1A, quantified by qPCR, left panel) and protein levels (representative western blot, middle panel; right panel represents the quantification of three independent western blots) in NHEK cells, 72 h after transfection with control (siCtrl) or two different *PPARD* siRNAs (siPPARD D, siPPARD 2). GAPDH was used as a loading control. (D) Cell proliferation quantified by EdU uptake and FACS analysis of the cell cycle in malignant keratinocytes SCC13 (left) and human A375 melanoma cells (right), 72 h after transfection with control (siCtrl) or a pool of four *PPARD* siRNAs (siPPARD pool). Bars represent mean ± standard deviation from at least three independent biological replicates (white circles), each with three technical replicates. (****$p < .0001$; ***$p < .001$; **$p < .01$; *$p < .05$, ns (non-significant) $p > .05$; two-tailed Student's *t*-test for two group comparisons, and one-way ANOVA with Dunnett's multiple-comparison test for more than two group comparisons).

it did not compensate for the increase in the expression of p21 due to PPARβ depletion, and the p21 levels remained higher than in control NHEK cells.

While DNA repair is the desired outcome of DDR, inefficient DDR has been demonstrated to elicit an increase in UV-induced apoptosis in human keratinocytes.[39,40] In line with our data suggesting impaired DDR response as a consequence of PPARβ depletion, we observed that UVB exposure induced almost two-folds more apoptosis in cells with PPARβ depletion as compared to control cells (17.7% ± 9.6 increase in apoptotic cells following UVB exposure in control cells (siCtrl pool), compared to 34.8% ± 13.4, and 30.9% ± 8.6 increase in siPPARD 2 and siPPARD D, respectively, after UV exposure. Figure 4D).

Here, we have shown that siRNA-mediated depletion of PPARβ in NHEK cells did not affect the induction of DNA damage following UV radiation, but rather compromised

the ability of cells to efficiently activate the DDR pathway upon UV-induced DNA damage. The reduced formation of γH2AX, activation of ATR pathway effector proteins, and p21 accumulation as a result of PPARβ depletion in human keratinocytes, all suggest a nonefficient DDR in response to UVB radiation, that leads to increased apoptotic response to UVB exposure in these cells (Figure 5).
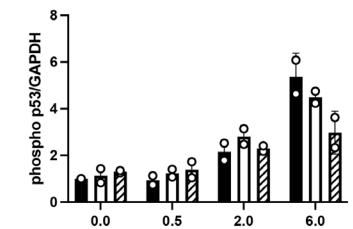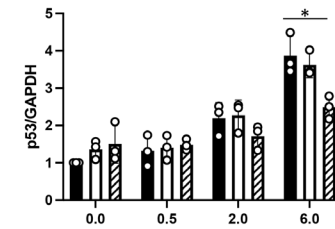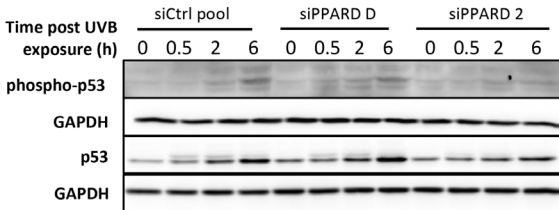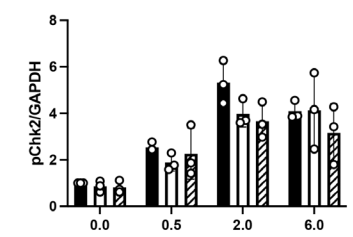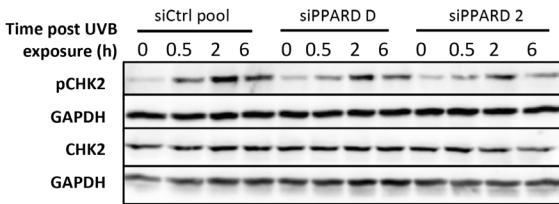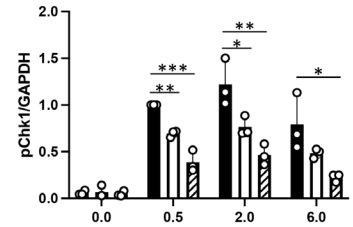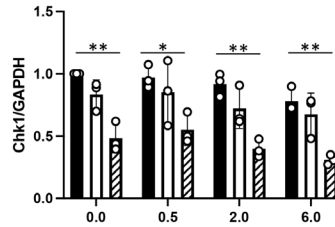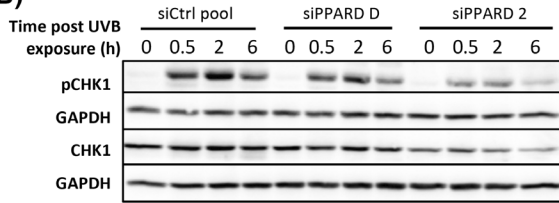
3.4 | Pharmacological inhibition of PPARβ in malignant human skin keratinocytes affects their cell cycle and response to UV exposure

The data presented in the current study of human keratinocytes, together with our previous observations that PPARβ knockout (KO) reduces the development of
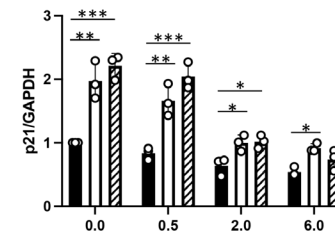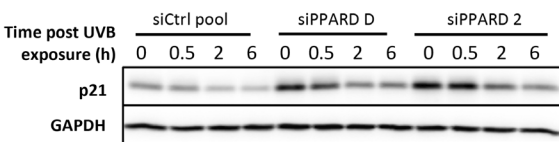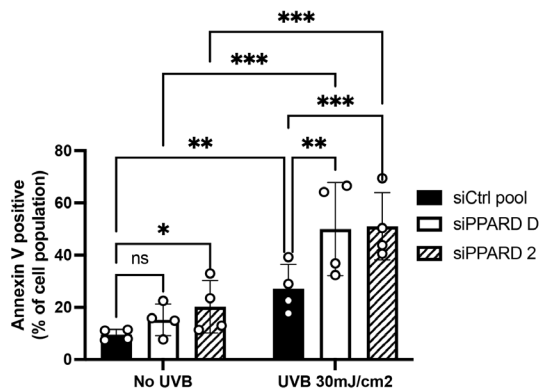
(A)
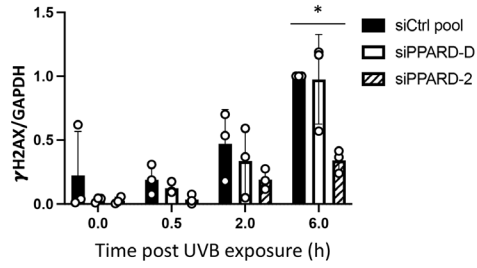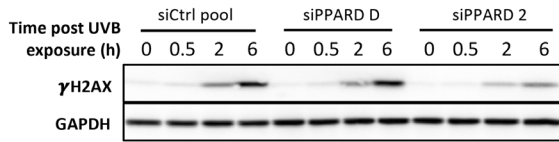
(B)
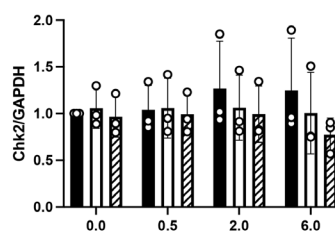
(C)

(D)

FIGURE 4 Effect of PPARβ depletion on human keratinocyte response to UV. Representative western blot (left) and quantification of three independent western blots (right) of phosphorylated (A) H2AX (γH2AX), (B) total and phosphorylated CHK1, CHK2, p53, and (C) p21 proteins at 0, 0.5, 2 and 6 h after UVB-exposure in PPARβ-depleted (siPPARD D, siPPARD 2) and control (siCtrl pool) NHEK cells. GAPDH levels were used as loading controls. (D) Percentage of apoptotic cells in response to UVB exposure (48 h post-exposure) using FACS analysis of Annexin V (as a marker for apoptosis) in PPARβ-depleted (siPPARD D, siPPARD 2) and control (siCtrl pool) NHEK cells. Bars represent mean ± standard deviation from at least two independent biological replicates (white circles), each with three technical replicates. (***$p < .001$; **$p < .01$; *$p < .05$, one-way ANOVA with Dunnett's multiple-comparison test for quantification of western blots, and two-way ANOVA with Tukey's multiple-comparison test for Annexin V FACS).
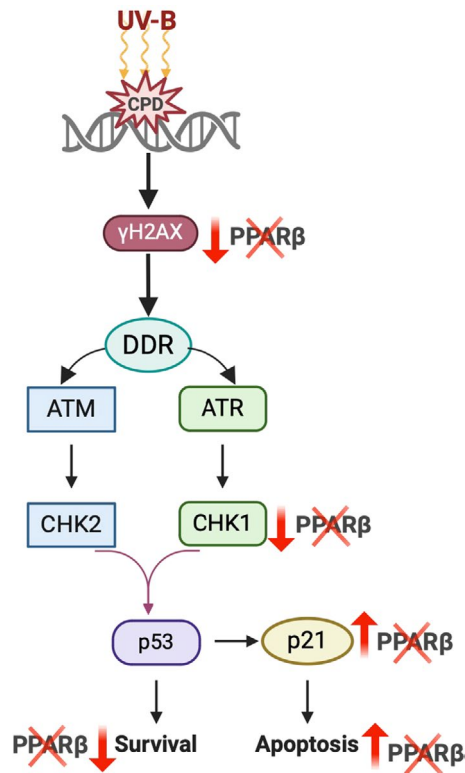

Created in BioRender. Jafari, P. (2024)
https://BioRender.com/z99b363

FIGURE 5 PPARβ depletion impairs DNA damage response. Schematic model illustrating the impact of PPARβ depletion on the DNA damage response (DDR) pathway and outcome.

UV-induced tumors in murine skin,[17] suggest that PPARβ depletion or loss-of-function, modulates the skin response to UV, probably by regulating DDR and increasing the apoptotic response of damaged cells, and by decreasing proliferation. As a member of the family of ligand-induced nuclear hormone receptors, PPARβ is a druggable transcription factor. Small molecules inducing or inhibiting its activity are available,[41,42] making PPARβ an interesting target candidate in the prevention or treatment of skin cancers. We thus assessed the effect of the pharmacological inhibition of PPARβ on cell proliferation and response to UVB exposure in human malignant keratinocytes isolated from human skin squamous cell carcinoma

lesions, namely SCC13 malignant keratinocyte cell line. To do so, we treated SCC13 cells with GSK0660, one of the best characterized PPARβ pharmacological inhibitors.[42] Similar to results obtained with siRNA-mediated depletion of PPARβ in NHEK cells (Figure 3), pharmacological inhibition of PPARβ in malignant human keratinocytes (SCC13) led to reduced proliferation (around $35 \pm 6\%$ reduction) and led to cell cycle arrest, concomitant with an increase in p21 expression (1.47 ± 0.08-fold increase in mRNA level and 2.44 ± 0.37-fold increase in protein level; Figure 6A,B). Also, in line with our data obtained in NHEK cells, we observed a decrease in the expression of proteins regulating cell proliferation, namely CHK1, E2F1 and PCNA, both at the RNA (Figure 6C, left panel) and protein (Figure 6C, right panel) levels in GSK0660-treated SCC13 cells compared to control (DMSO) cells. In response to UVB exposure, the phosphorylation, thereby activation, of H2AX and CHK1 was also lower in PPARβ-inhibited compared to control SCC13 cells (Figure 6D, upper and middle panels, respectively). Pharmacological inhibition of PPARβ with GSK0660 also induced a strong increase in p21 protein expression, which level remained higher in these GSK0660-treated SCC13 cells compared to control SCC13 cells following UV exposure (Figure 6D, lower panel). Finally, the apoptotic response of SSC13 cells to UV was also significantly increased in PPARβ-inhibited SCC13 cells compared to control cells ($58.1 \pm 4.7\%$ increase in apoptotic cells following UVB exposure in control cells (DMSO), compared to $69.3 \pm 2.4\%$ in PPARβ inhibited cells (GSK0660)) (Figure 6E). Thus, pharmacological inhibition of PPARβ is also effective in regulating cellular proliferation and UV response in malignant keratinocytes, similar to PPARβ depletion in healthy keratinocytes.

## 3.5 | PPARβ could be a potential target for prevention or treatment of skin cancers

Our results in cultured normal (NHEK) and malignant (SCC13) human keratinocytes demonstrate the role of PPARβ as a regulator of cell cycle and response to UV exposure. We also showed that pharmacological inhibition of PPARβ activity can alter the proliferation of human

(A)

(B)

(C)

(D)

(E)
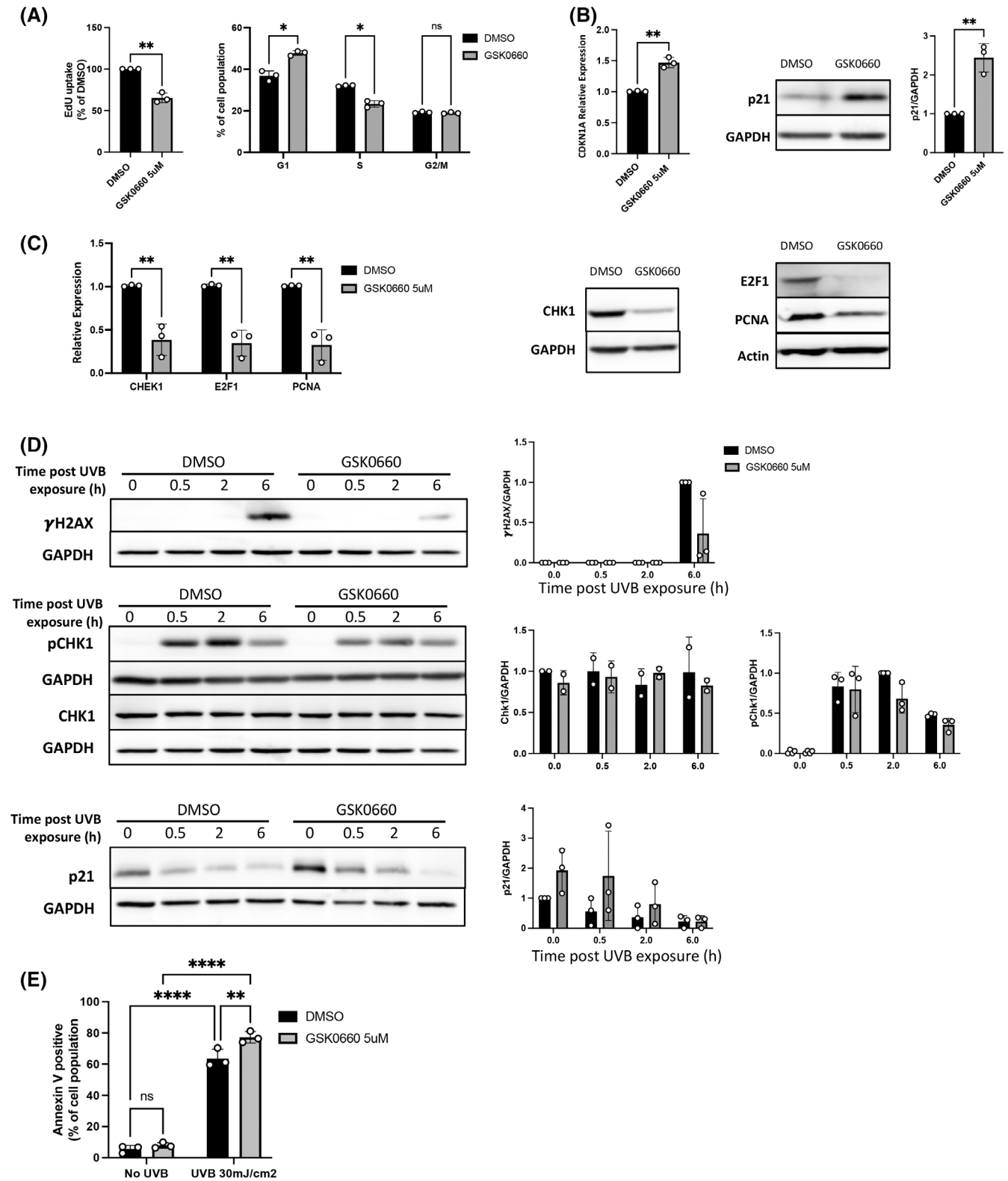
skin squamous cell carcinoma cells (SCC13). To gain further insights into the potential of PPARβ as a drug target, we questioned PPARβ expression levels in patient tumors. Datasets being unfortunately not available for squamous cell carcinoma in public databases, we extended our investigation to the most-deadly skin cancer, that is, melanoma.

We analyzed the levels of PPARD mRNA transcripts in two independent TCGA melanoma cohorts using the R2 platform (microarray analysis and visualization platform; http://r2.amc.nl, University of Amsterdam). In these cohorts of 375 and 470 skin melanoma samples (R2 IDs: TCGA-375-rsem-tcgars (Figure 7A, up), and

FIGURE 6 Effect of pharmacological inhibition of PPARβ in malignant human keratinocytes (SCC13). (A) Cell proliferation quantified using EdU uptake (left) and FACS analysis of the cell cycle progression (right) in control (DMSO) and PPARβ-inhibited (GSK0660) malignant human keratinocytes (SCC13). (B) Expression of p21 at mRNA (CDKA1A, quantified by qPCR; left) and protein (representative western blot, middle panel; right panel represents the quantification of three independent western blots) in control (DMSO) and PPARβ-inhibited (GSK0660) SCC13 cells. (C) Expression of CHK1, E2F1 and PCNA at the mRNA (qPCR) and protein levels (western blot) in control (DMSO) and PPARβ-inhibited (GSK0660) SCC13 cells. (D) Representative western blots (left) and quantification of three independent western blots (right) of phosphorylated H2AX (γH2AX) (upper panel), of total and phosphorylated CHK1 (middle panels), and of p21 at 0, 0.5, 2, and 6 h after UVB-exposure in control (DMSO) and PPARβ-inhibited (GSK0660) SCC13 cells. (E) Percentage of apoptotic cells in response to UVB exposure using FACS analysis of Annexin V on control (DMSO) and PPARβ-inhibited (GSK0660) SCC13 cells. Actin and GAPDH have been used as loading controls. Bars represent mean ± standard deviation from three independent biological replicates (white circles), each with three technical replicates (panels A–C, and E). For western blots (panel D), each white circle corresponds to one independent experiment ($n = 3$). (****$p < .0001$; **$p < .01$; *$p < .05$, two-tailed Student's t-test for two group comparisons, and two-way ANOVA with Tukey's multiple-comparison test for Annexin V FACS).
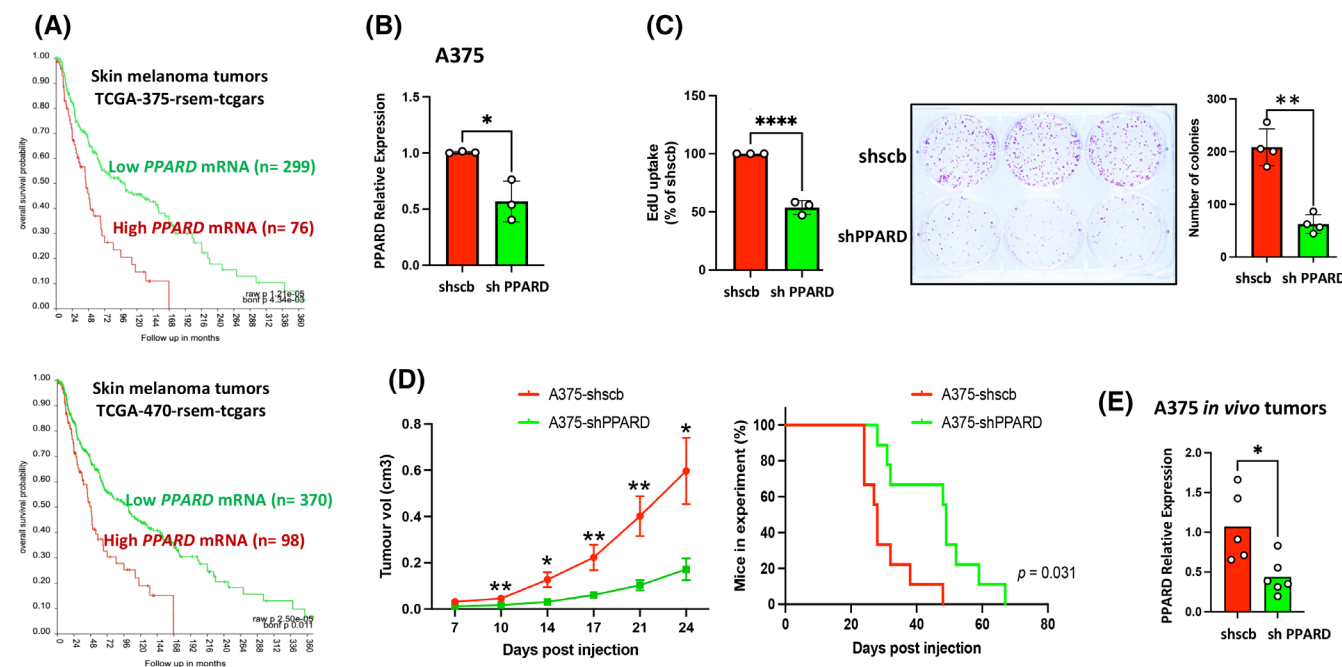
FIGURE 7 PPARβ depletion reduces the growth of melanoma tumors in a mouse xenograft model in vivo. (A) Kaplan–Meier survival curves demonstrating an association between patient survival and PPARβ expression levels in two TCGA melanoma cohorts with 375 (up), and 470 (bottom) melanoma tumors. (B) Expression of *PPARD* mRNA in A375 human melanoma cells infected with lentivirus expressing sham shRNA (shscb; control) or shRNA targeting *PPARD* (shPPAR D). (C) Proliferation (measured by EdU uptake; left) and colony formation (right) of control (shscb) or PPARβ-depleted (shPPARD) A375 human melanoma cells, prior to xenografting to mice. Bars represent mean ± standard deviation from at least three independent biological replicates (white circles), each with three technical replicates. (****$p < .0001$; **$p < .01$; *$p < .05$, two-tailed Student's t test). (D) Control (A375-shscb) or PPARβ-depleted (A375-shPPARD) A375 human melanoma cells were injected subcutaneously to 5–6 mice per experimental group and monitored for tumor growth. Tumor growth over time represented by quantification of tumor volume (in cm³; left), and the number of animals remained in the study during a 70-day observation period (**$p < .01$; *$p < .05$). (E) Expression of *PPARD* mRNA in tumors (one tumor per mouse) isolated from mice xenografted with A375-shscb (control; $n = 5$ mice) or A375-shPPARD ($n = 6$ mice) melanoma cells. Each white circles represents one tumor. (*$p < .05$, two-tailed Student's t test).

TCGA-470-rsem-tcgars (Figure 7A, down)), lower PPARβ expression was significantly associated with higher overall patient survival. We therefore tested the effect of PPARβ depletion on the tumorigenicity of invasive human melanoma A375 cells. PPARβ depletion (shRNA-mediated; 0.53 ± 0.06-fold reduction in expression; Figure 7B) in

A375 cells provoked a similar antiproliferative effect as in human primary and malignant keratinocytes (46 ± 0.06% reduction in EdU uptake; Figure 7C, left). Also, PPARβ-depleted A375 cells showed strongly reduced colony forming potential as tested by clonogenic assay (0.3 ± 0.09-fold reduction in number of colonies; Figure 7C, right).

Using an in vivo model of human melanoma xenografts in nude mice, we show that stable shRNA-mediated depletion of PPARβ in A375 melanoma cells (shPPARD), reduced tumor volume in vivo, as compared with PPARβ-proficient control cells (shscb; 0.44 ± 0.23-fold reduction in tumor volume) that formed significantly larger tumors (Figure 7E, left panel). Moreover, mice with PPARβ-proficient A375 tumors fulfilled the criteria for withdrawal from the experiment (experimental endpoint; tumor size 1 cm^3) earlier than those with tumors grown from PPARβ-deficient A375 cells (Figure 7D, right panel). The stable reduction in PPARβ expression in the melanoma tumor cells following tumor resection at the end of the experiment was confirmed by qPCR (Figure 7E). These results suggest that PPARβ has a potential as a drug target not only in squamous cell carcinoma but also in human melanoma.

4 | DISCUSSION

In this study, we report on the critical role of the PPARβ transcription factor in regulating cell cycle and proliferation, as well as cellular responses to UV exposure in cultured human epidermal cells. Using an in vivo xenograft melanoma model, we also show that inhibition of PPARβ expression reduces melanoma tumor growth, suggesting a potential for PPARβ inhibition as a therapeutic approach in human skin cancers.

4.1 | PPARβ regulates cell cycle and proliferation of human keratinocytes

To date, several studies report on the regulation of cell cycle and proliferation by PPARβ, but its function appears cell type and context dependent,[43] and there is no consensus on the involved mechanisms. Focusing on human skin cells, most of the available data relies on the experimental settings with induced activation or increased expression of PPARβ, for which the physiologically relevant setup is not easily achievable. Briefly, these studies report that ligand activation and/or overexpression of PPARβ inhibits proliferation and blocks progression of the cell cycle in human healthy or malignant keratinocytes, or in human melanoma cells.[44–46] Other studies report that, ligand activation of PPARβ in human primary keratinocytes boost proliferation, while in the same study, RNAi-mediated PPARβ depletion in immortalized keratinocytes led to a block in cell proliferation.[47] Based on a global analysis of the transcriptome, our study is the first to show that the expression of numerous genes associated with cell cycle progression and checkpoints, and DNA synthesis and elongation, are strongly repressed in PPARβ-depleted human healthy

keratinocytes. We show that these changes at the transcriptome level are well reflected at the functional level, since the proliferation of PPARβ-depleted human keratinocytes is indeed decreased and their cell cycle affected. We explain this PPARβ-dependent regulation of proliferation and cell cycle by the regulation of several gene families, that is, the MCM family and regulators of cell cycle progression. The MCM gene family consists of six gene products, MCM2-7,[23] and CDC45[48] which are essential components of the DNA helicase and are required for both DNA replication initiation and elongation at the S phase of cell cycle. Like we observe with PPARβ depletion, which resulted in a strong reduction in the expression of these genes, siRNA-mediated downregulation of MCM protein family was also shown to provoke G1/S cell cycle arrest, along with the accumulation of DNA lesions and induction of apoptotic response.[49] The expression of Cyclin B1 (CCNB1) and CDC25B genes, which are essential regulators of G2/M transition,[50,51] as well as the regulator of mitotic exit Cell division cycle 20 (CDC20),[52,53] was also reduced in PPARβ-depleted human keratinocytes. In line with our data, Cyclin B1 depletion leads to reduced proliferation and increased apoptosis in human tumor cells,[54] and a 40% downregulation of CDC25B mRNA in human primary keratinocytes blocks the EGF-induced proliferation.[55] Reinforcing the downregulation of these proteins, that promote cell cycle progression, we describe a significant upregulation of the cyclin-dependent kinase inhibitor protein 1, p21, at mRNA and protein levels following PPARβ depletion. p21 protein is a major inhibitor of cell cycle, that also regulates DDR, apoptosis, and senescence.[26] Regulation of p21 expression by PPARβ is still very poorly characterized. The activation of PPARβ in human retinal epithelial cells,[56] human vascular smooth muscle cells (VSMCs),[57] and in human coronary artery endothelial cells[58] inhibited senescence through inhibition of p21 upregulation. In murine aortic muscle cells and rat VSMCs, PPARβ activation led to the induction of p21 expression and antiproliferative effects.[59,60] In line with data showing that increased expression of p21 leads to cell cycle arrest at G2/M phase,[61] we observed that PPARβ-depleted human keratinocytes failed to progress into the cell cycle and accumulated in G2/M phase. In summary, we show that reducing PPARβ expression in human skin cells blocks proliferation and the cell cycle, which presumably involves PPARβ-dependent regulation of several key cell cycle regulators.

4.2 | PPARβ regulates DNA repair and UV response of human keratinocytes

Our RNA-seq data also revealed that genes involved in DNA repair pathways are among the most affected upon

PPARβ depletion in normal human keratinocytes, showing a general repression in their expression. Among them, the Fanconi Anemia/BRCA (FA/BRCA) pathway genes are of major interest in the context of the skin responses to UV. The FA/BRCA pathway protects against genomic instability by coordinating several distinct repair mechanisms including nucleotide excision repair (NER), and homologous recombination (HR) in response to DNA damaging agents including UV radiation.[62,63] PPARβ depletion in normal human keratinocytes caused a significant decrease in the expression of multiple genes in this pathway, namely FANCA, FANCD2, FANKI, and BRCA2. Considering the central role of FA pathway in DNA repair, it is plausible that the PPARβ-depleted cells are less competent in coping with DNA-damaging agents including UV radiation, which is of major significance in the development of skin cancers.[1] We therefore investigated the response of PPARβ-depleted keratinocytes to UV radiation. We showed that PPARβ depletion or its pharmacological inhibition indeed alters the expression and activation of multiple proteins with crucial functions at different steps of DDR. Among those, PPARβ depletion led to a significant decrease in the formation of γH2AX and pCHK1 in normal human keratinocytes in response to UVB exposure. γH2AX protein functions as a platform for the recruitment of DNA repair factors and initiation of DDR.[64] It has been shown that reduced expression and formation of γH2AX increases the cellular sensitivity to DNA-damaging agents and promotes the apoptotic response to DNA damage in these cells.[65–67] A similar effect has been reported for CHK1, in which its downregulation increases the cellular sensitivity to DNA-damaging stimuli, leading to cellular apoptosis.[68] In line with these reported consequences of reduced activation of H2AX and CHK1, we demonstrate that PPARβ depletion eventually increased the apoptotic response to UV-induced DNA damage in normal human keratinocytes. p21, in addition to its role as a cell-cycle inhibitor described above, is also involved in modulating DDR via regulating proliferating cell nuclear antigen (PCNA) interactions with multiple DNA repair factors.[35,36] Stable expression of p21 following UV-induced DNA damage can block PCNA function in DNA repair.[69] Moreover, UV-induced and ATR-dependent degradation of p21 is essential for DNA damage repair.[37] Here we observe that when normal human keratinocytes are exposed to UVB, p21 protein levels decline over time as expected.[37] This reduction in p21 is also observed in PPARβ-depleted NHEK cells however, as p21 expression is strongly increased in PPARβ-depleted cells, the level of p21 expression remains abnormally high, which likely contributes to compromised functioning of DDR. Finally, p53 is another important effector protein in DDR pathway,[70] that showed a significant reduction upon an 80% downregulation of

PPARβ with one of the siRNA constructs. Collectively, the altered expression and activation of several proteins of the DDR pathway (e.g., H2AX, CHK1, p21, p53) that we report here, can explain the increased apoptotic response that we observe in PPARβ-depleted cells to UV radiation.

4.3 | PPARβ as a therapeutic target

Combined with our published study showing that PPARβ KO reduces the formation of UV-induced cutaneous carcinoma in mice,[17] the findings in the present study show that PPARβ-depletion acts as an inhibitor of human skin cell proliferation, as a regulator of cellular response to UV and as an activator of apoptosis, warrants for considering PPARβ inhibition as a therapeutic strategy for the prevention or treatment of skin cancers. In addition to blocking the proliferation of cancer cells, therapeutic strategies targeting DNA repair in cancer cells are of major clinical interest.[71] Alterations in the efficiency of DDR enhance the efficacy of genotoxic anti-cancer therapies by preventing DNA repair and increasing the rate of apoptosis in cancer cells.[72,73] It is interesting to note that PPARβ depletion covers all the above-mentioned mechanisms and could thus increase the chances of the eradication of human epidermal cancer cells. In addition to malignant cells of keratinocyte origin (SCC13), we show that PPARβ-depletion in invasive melanoma cell lines too, reduces their proliferative capacity. Permanent lentiviral shRNA-mediated depletion of PPARβ in A375 melanoma cells significantly reduced their tumorigenicity cells in an in vivo model of human melanoma cell xenografts in nude mice. This strong evidence supports the translational value of PPARβ inhibition as a preventive or therapeutic strategy for human cancers with epidermal origin, considering the availability of direct pharmacological activators and inhibitors of PPARβ activity.[74] Obviously, minimizing the side effects of the PPARβ inhibition on healthy skin keratinocytes should be considered while designing the delivery method of PPARβ inhibitors. Nevertheless, skin cancers being the target of the PPARβ inhibition strategy makes the concern of side effects less of a challenge, because of the possibility of targeted topical delivery of pharmacological small molecules to skin.

The controversial role of PPARβ in promoting or inhibiting proliferation and tumorigenesis for different cell lines from human cancers with epithelial origin (colon, lung, breast), and mice models have been reported.[75] With regard to skin cancers, there are reports of the antiproliferative effect of the ligand activation or overexpression of PPARβ in human melanoma cells.[46,76] For skin cancers of keratinocyte origin (skin SCC), the main body of evidence is acquired by

in vivo studies on PPARβ KO mice, with conflicting outcomes that can be attributed to the method used to induce tumor development (chemically, DMBA/TPA-induced[77] vs. UV-induced carcinogenesis).[17] In the context of the etiology of skin cancers of keratinocyte origin, chronic UV exposure being more relevant as the induction factor for carcinogenesis, we showed that PPARβ KO mice develop fewer and less severe SCC lesions in response to UV.[17] With regards to human skin response to UV, the data we present in this study in human epidermal cells suggest a parallel with what we have observed in mice and propose a mechanism of action of PPARβ in human skin exposed to UV.

AUTHOR CONTRIBUTIONS

ACKNOWLEDGMENTS

FUNDING INFORMATION

DISCLOSURES

The authors declare they have no conflict of interests.

DATA AVAILABILITY STATEMENT

Datasets related to this article can be found in NCBI Gene Expression Omnibus (GEO; http://www.ncbi.nlm.nih.gov/geo/; Edgar et al. 2002)[78] and are accessible through GEO series accession number GSE263846 (https://www.ncbi.nlm.nih.gov/geo/query/acc.cgi?acc=GSE263846).

ORCID

Thanh Nhan Nguyen https://orcid.org/0009-0001-6923-8370
Stéphanie Claudinot https://orcid.org/0000-0002-0190-1586
Liliane Michalik https://orcid.org/0000-0003-2963-2100
Paris Jafari https://orcid.org/0000-0003-1656-9480

REFERENCES

1. Narayanan DL, Saladi RN, Fox JL. Ultraviolet radiation and skin cancer. *Int J Dermatol*. 2010;49(9):978-986.
2. Helt CE, Cliby WA, Keng PC, Bambara RA, O'Reilly MA. Ataxia telangiectasia mutated (ATM) and ATM and Rad3-related protein exhibit selective target specificities in response to different forms of DNA damage. *J Biol Chem*. 2005;280(2):1186-1192.
3. Hafner A, Bulyk ML, Jambhekar A, Lahav G. The multiple mechanisms that regulate p53 activity and cell fate. *Nat Rev Mol Cell Biol*. 2019;20(4):199-210.
4. Nowsheen S, Yang ES. The intersection between DNA damage response and cell death pathways. *Exp Oncol*. 2012;34(3):243-254.
5. Hu J, Adar S, Selby CP, Lieb JD, Sancar A. Genome-wide analysis of human global and transcription-coupled excision repair of UV damage at single-nucleotide resolution. *Genes Dev*. 2015;29(9):948-960.
6. Roos WP, Thomas AD, Kaina B. DNA damage and the balance between survival and death in cancer biology. *Nat Rev Cancer*. 2016;16(1):20-33.
7. Jackson SP, Bartek J. The DNA-damage response in human biology and disease. *Nature*. 2009;461(7267):1071-1078.
8. Toledo LI, Murga M, Zur R, et al. A cell-based screen identifies ATR inhibitors with synthetic lethal properties for cancer-associated mutations. *Nat Struct Mol Biol*. 2011;18(6):721-727.
9. Szydzik J, Lind DE, Arefin B, et al. ATR inhibition enables complete tumour regression in ALK-driven NB mouse models. *Nat Commun*. 2021;12(1):6813.
10. Gralewska P, Gajek A, Marczak A, et al. PARP inhibition increases the reliance on ATR/CHK1 checkpoint signaling leading to synthetic lethality-an alternative treatment strategy for epithelial ovarian cancer cells independent from HR effectiveness. *Int J Mol Sci*. 2020;21(24):9715.
11. Wang Y, Nakajima T, Gonzalez FJ, Tanaka N. PPARs as metabolic regulators in the liver: lessons from liver-specific PPAR-null mice. *Int J Mol Sci*. 2020;21(6):2061.
12. Tan NS, Michalik L, Noy N, et al. Critical roles of PPAR beta/delta in keratinocyte response to inflammation. *Genes Dev*. 2001;15(24):3263-3277.
13. Di-Poi N, Tan NS, Michalik L, Wahli W, Desvergne B. Antiapoptotic role of PPARbeta in keratinocytes via transcriptional control of the Akt1 signaling pathway. *Mol Cell*. 2002;10(4):721-733.
14. Tan NS, Icre G, Montagner A, Bordier-ten-Heggeler B, Wahli W, Michalik L. The nuclear hormone receptor peroxisome proliferator-activated receptor beta/delta potentiates cell chemotactism, polarization, and migration. *Mol Cell Biol*. 2007;27(20):7161-7175.
15. Chong HC, Tan MJ, Philippe V, et al. Regulation of epithelial-mesenchymal IL-1 signaling by PPARbeta/delta is essential for skin homeostasis and wound healing. *J Cell Biol*. 2009;184(6):817-831.
16. Tan NS, Michalik L, Desvergne B, Wahli W. Genetic- or transforming growth factor-beta 1-induced changes in

epidermal peroxisome proliferator-activated receptor beta/delta expression dictate wound repair kinetics. *J Biol Chem*. 2005;280(18):18163-18170.

17. Montagner A, Delgado MB, Tallichet-Blanc C, et al. Src is activated by the nuclear receptor peroxisome proliferator-activated receptor beta/delta in ultraviolet radiation-induced skin cancer. *EMBO Mol Med*. 2014;6(1):80-98.

18. Serrels B, Serrels A, Mason SM, et al. A novel Src kinase inhibitor reduces tumour formation in a skin carcinogenesis model. *Carcinogenesis*. 2009;30(2):249-257.

19. Ciazynska M, Olejniczak-Staruch I, Sobolewska-Sztychny D, Narbutt J, Skibinska M, Lesiak A. Ultraviolet radiation and chronic inflammation-molecules and mechanisms involved in skin carcinogenesis: a narrative review. *Life (Basel)*. 2021;11(4):326.

20. Degueurce G, D'Errico I, Pich C, et al. Identification of a novel PPARbeta/delta/miR-21-3p axis in UV-induced skin inflammation. *EMBO Mol Med*. 2016;8(8):919-936.

21. Salmon P, Trono D. Production and titration of lentiviral vectors. *Curr Protoc Neurosci*. 2006;53(1):4-21.

22. Ren B, Cam H, Takahashi Y, et al. E2F integrates cell cycle progression with DNA repair, replication, and G(2)/M checkpoints. *Genes Dev*. 2002;16(2):245-256.

23. Davey MJ, Indiani C, O'Donnell M. Reconstitution of the Mcm2-7p heterohexamer, subunit arrangement, and ATP site architecture. *J Biol Chem*. 2003;278(7):4491-4499.

24. Hydbring P, Malumbres M, Sicinski P. Non-canonical functions of cell cycle cyclins and cyclin-d ependent kinases. *Nat Rev Mol Cell Biol*. 2016;17(5):280-292.

25. Asghar U, Witkiewicz AK, Turner NC, Knudsen ES. The history and future of targeting cyclin-dependent kinases in cancer therapy. *Nat Rev Drug Discov*. 2015;14(2):130-146.

26. Engeland K. Cell cycle regulation: p53-p21-RB signaling. *Cell Death Differ*. 2022;29(5):946-960.

27. Kciuk M, Marciniak B, Mojzych M, Kontek R. Focus on UV-induced DNA damage and repair-disease relevance and protective strategies. *Int J Mol Sci*. 2020;21(19):7264.

28. Mah LJ, El-Osta A, Karagiannis TC. gammaH2AX: a sensitive molecular marker of DNA damage and repair. *Leukemia*. 2010;24(4):679-686.

29. Shiloh Y, Ziv Y. The ATM protein kinase: regulating the cellular response to genotoxic stress, and more. *Nat Rev Mol Cell Biol*. 2013;14(4):197-210.

30. Lee JW, Ratnakumar K, Hung KF, Rokunohe D, Kawasumi M. Deciphering UV-induced DNA damage responses to prevent and treat skin cancer. *Photochem Photobiol*. 2020;96(3):478-499.

31. Zhou BB, Elledge SJ. The DNA damage response: putting checkpoints in perspective. *Nature*. 2000;408(6811):433-439.

32. Stokes MP, Rush J, Macneill J, et al. Profiling of UV-induced ATM/ATR signaling pathways. *Proc Natl Acad Sci USA*. 2007;104(50):19855-19860.

33. Bartek J, Lukas J. Chk1 and Chk2 kinases in checkpoint control and cancer. *Cancer Cell*. 2003;3(5):421-429.

34. Loughery J, Cox M, Smith LM, Meek DW. Critical role for p53-serine 15 phosphorylation in stimulating transactivation at p53-responsive promoters. *Nucleic Acids Res*. 2014;42(12):7666-7680.

35. Ticli G, Cazzalini O, Stivala LA, Prosperi E. Revisiting the function of p21(CDKN1A) in DNA repair: the influence of protein interactions and stability. *Int J Mol Sci*. 2022;23(13):7058.

36. Abbas T, Dutta A. p21 in cancer: intricate networks and multiple activities. *Nat Rev Cancer*. 2009;9(6):400-414.

37. Bendjennat M, Boulaire J, Jascur T, et al. UV irradiation triggers ubiquitin-dependent degradation of p21(WAF1) to promote DNA repair. *Cell*. 2003;114(5):599-610.

38. Soria G, Speroni J, Podhajcer OL, Prives C, Gottifredi V. p21 differentially regulates DNA replication and DNA-repair-associated processes after UV irradiation. *J Cell Sci*. 2008;121(Pt 19):3271-3282.

39. Heffernan TP, Kawasumi M, Blasina A, Anderes K, Conney AH, Nghiem P. ATR-Chk1 pathway inhibition promotes apoptosis after UV treatment in primary human keratinocytes: potential basis for the UV protective effects of caffeine. *J Invest Dermatol*. 2009;129(7):1805-1815.

40. Shaj K, Hutcherson RJ, Kemp MG. ATR kinase activity limits mutagenesis and promotes the Clonogenic survival of quiescent human keratinocytes exposed to UVB radiation. *Photochem Photobiol*. 2020;96(1):105-112.

41. Sznaidman ML, Haffner CD, Maloney PR, et al. Novel selective small molecule agonists for peroxisome proliferator-activated receptor delta (PPARdelta)--synthesis and biological activity. *Bioorg Med Chem Lett*. 2003;13(9):1517-1521.

42. Shearer BG, Steger DJ, Way JM, et al. Identification and characterization of a selective peroxisome proliferator-activated receptor beta/delta (NR1C2) antagonist. *Mol Endocrinol*. 2008;22(2):523-529.

43. Muller R, Rieck M, Muller-Brusselbach S. Regulation of cell proliferation and differentiation by PPARbeta/delta. *PPAR Res*. 2008;2008:614852.

44. Burdick AD, Bility MT, Girroir EE, et al. Ligand activation of peroxisome proliferator-activated receptor-beta/delta(PPARbeta/delta) inhibits cell growth of human N/TERT-1 keratinocytes. *Cell Signal*. 2007;19(6):1163-1171.

45. Borland MG, Kehres EM, Lee C, et al. Inhibition of tumorigenesis by peroxisome proliferator-activated receptor (PPAR)-dependent cell cycle blocks in human skin carcinoma cells. *Toxicology*. 2018;404–405:25-32.

46. Borland MG, Yao PL, Kehres EM, et al. Editor's highlight: PPARbeta/delta and PPARgamma inhibit melanoma Tumorigenicity by modulating inflammation and apoptosis. *Toxicol Sci*. 2017;159(2):436-448.

47. Romanowska M, Al Yacoub N, Seidel H, et al. PPARdelta enhances keratinocyte proliferation in psoriasis and induces heparin-binding EGF-like growth factor. *J Invest Dermatol*. 2008;128(1):110-124.

48. Simon AC, Sannino V, Costanzo V, Pellegrini L. Structure of human Cdc45 and implications for CMG helicase function. *Nat Commun*. 2016;7:11638.

49. Ibarra A, Schwob E, Mendez J. Excess MCM proteins protect human cells from replicative stress by licensing backup origins of replication. *Proc Natl Acad Sci USA*. 2008;105(26):8956-8961.

50. Morgan DO. Principles of CDK regulation. *Nature*. 1995;374(6518):131-134.

51. Lammer C, Wagerer S, Saffrich R, Mertens D, Ansorge W, Hoffmann I. The cdc25B phosphatase is essential for the G2/M phase transition in human cells. *J Cell Sci*. 1998;111(pt 16):2445-2453.

52. Kapanidou M, Curtis NL, Bolanos-Garcia VM. Cdc20: at the crossroads between chromosome segregation and mitotic exit. *Trends Biochem Sci*. 2017;42(3):193-205.

53. Yu H. Cdc20: a WD40 activator for a cell cycle degradation machine. *Mol Cell*. 2007;27(1):3-16.

54. Yuan J, Yan R, Kramer A, et al. Cyclin B1 depletion inhibits proliferation and induces apoptosis in human tumor cells. *Oncogene*. 2004;23(34):5843-5852.

55. Hsieh WL, Lin YK, Tsai CN, Wang TM, Chen TY, Pang JH. Indirubin, an acting component of indigo naturalis, inhibits EGFR activation and EGF-induced CDC25B gene expression in epidermal keratinocytes. *J Dermatol Sci*. 2012;67(2):140-146.

56. Lee EJ, Won JP, Lee HG, et al. PPARdelta inhibits hyperglycemia-triggered senescence of retinal pigment epithelial cells by up-regulating SIRT1. *Antioxidants (Basel)*. 2022;11(6):1207.

57. Kim HJ, Ham SA, Kim MY, et al. PPARdelta coordinates angiotensin II-induced senescence in vascular smooth muscle cells through PTEN-mediated inhibition of superoxide generation. *J Biol Chem*. 2011;286(52):44585-44593.

58. Kim MY, Kang ES, Ham SA, et al. The PPARdelta-mediated inhibition of angiotensin II-induced premature senescence in human endothelial cells is SIRT1-dependent. *Biochem Pharmacol*. 2012;84(12):1627-1634.

59. Sue YM, Chung CP, Lin H, et al. PPARdelta-mediated p21/p27 induction via increased CREB-binding protein nuclear translocation in beraprost-induced antiproliferation of murine aortic smooth muscle cells. *Am J Physiol Cell Physiol*. 2009;297(2):C321-C329.

60. Kim HJ, Kim MY, Hwang JS, et al. PPARdelta inhibits IL-1beta-stimulated proliferation and migration of vascular smooth muscle cells via up-regulation of IL-1Ra. *Cell Mol Life Sci*. 2010;67(12):2119-2130.

61. Bunz F, Dutriaux A, Lengauer C, et al. Requirement for p53 and p21 to sustain G2 arrest after DNA damage. *Science*. 1998;282(5393):1497-1501.

62. Walden H, Deans AJ. The Fanconi anemia DNA repair pathway: structural and functional insights into a complex disorder. *Annu Rev Biophys*. 2014;43:257-278.

63. Dunn J, Potter M, Rees A, Runger TM. Activation of the Fanconi anemia/BRCA pathway and recombination repair in the cellular response to solar ultraviolet light. *Cancer Res*. 2006;66(23):11140-11147.

64. Fernandez-Capetillo O, Lee A, Nussenzweig M, Nussenzweig A. H2AX: the histone guardian of the genome. *DNA Repair (Amst)*. 2004;3(8–9):959-967.

65. Yaglom JA, McFarland C, Mirny L, Sherman MY. Oncogene-triggered suppression of DNA repair leads to DNA instability in cancer. *Oncotarget*. 2014;5(18):8367-8378.

66. Gruosso T, Mieulet V, Cardon M, et al. Chronic oxidative stress promotes H2AX protein degradation and enhances chemosensitivity in breast cancer patients. *EMBO Mol Med*. 2016;8(5):527-549.

67. Lal A, Pan Y, Navarro F, et al. miR-24-mediated downregulation of H2AX suppresses DNA repair in terminally differentiated blood cells. *Nat Struct Mol Biol*. 2009;16(5):492-498.

68. Xiao Z, Xue J, Sowin TJ, Rosenberg SH, Zhang H. A novel mechanism of checkpoint abrogation conferred by Chk1 down-regulation. *Oncogene*. 2005;24(8):1403-1411.

69. Soria G, Podhajcer O, Prives C, Gottifredi V. P21Cip1/WAF1 downregulation is required for efficient PCNA ubiquitination after UV irradiation. *Oncogene*. 2006;25(20):2829-2838.

70. Meek DW. Tumour suppression by p53: a role for the DNA damage response? *Nat Rev Cancer*. 2009;9(10):714-723.

71. Choi W, Lee ES. Therapeutic targeting of DNA damage response in cancer. *Int J Mol Sci*. 2022;23(3):1701.

72. Pilie PG, Tang C, Mills GB, Yap TA. State-of-the-art strategies for targeting the DNA damage response in cancer. *Nat Rev Clin Oncol*. 2019;16(2):81-104.

73. Huang R, Zhou PK. DNA damage repair: historical perspectives, mechanistic pathways and clinical translation for targeted cancer therapy. *Signal Transduct Target Ther*. 2021;6(1):254.

74. Grygiel-Gorniak B. Peroxisome proliferator-activated receptors and their ligands: nutritional and clinical implications—a review. *Nutr J*. 2014;13:13-17.

75. Wagner N, Wagner KD. PPAR Beta/Delta and the hallmarks of cancer. *Cells*. 2020;9(5):1133.

76. Michiels JF, Perrin C, Leccia N, Massi D, Grimaldi P, Wagner N. PPARbeta activation inhibits melanoma cell proliferation involving repression of the Wilms' tumour suppressor WT1. *Pflugers Arch*. 2010;459(5):689-703.

77. Bility MT, Devlin-Durante MK, Blazanin N, et al. Ligand activation of peroxisome proliferator-activated receptor beta/delta (PPAR beta/delta) inhibits chemically induced skin tumorigenesis. *Carcinogenesis*. 2008;29(12):2406-2414.

78. Edgar R, Domrachev M, Lash AE. Gene Expression Omnibus: NCBI gene expression and hybridization array data repository. *Nucleic Acids Res*. 2002;30(1):207-10.

SUPPORTING INFORMATION

Additional supporting information can be found online in the Supporting Information section at the end of this article.